Atmos. Chem. Phys. Discuss., 12, 5771–5801, 2012
www.atmos-chem-phys-discuss.net/12/5771/2012/
doi:10.5194/acpd-12-5771-2012

Atmospheric Chemistry and Physics Discussions

Diurnal tracking of anthropogenic CO_2 emissions in the Los Angeles basin megacity during spring, 2010

S. Newman[1], S. Jeong[2], M. L. Fischer[2], X. Xu[3], C. L. Haman[4], B. Lefer[4], S. Alvarez[4], B. Rappenglueck[4], E. A. Kort[5], A. E. Andrews[6], J. Peischl[7], K. R. Gurney[8], C. E. Miller[9], and Y. L. Yung[1]

[1]Division of Geological and Planetary Sciences, California Institute of Technology, Pasadena, CA 91125, USA
[2]Atmospheric Science Department, Lawrence Berkeley National Laboratory, MS 90K-125, 1 Cyclotron Rd., Berkeley, CA, 94720, USA
[3]Department of Earth System Science, University of California, Irvine, CA 92697, USA
[4]Department of Earth and Atmospheric Sciences, The University of Houston, 4800 Calhoun Road, Houston, Texas 77004, USA
[5]Jet Propulsion Laboratory, 4800 Oak Grove Drive, Pasadena, CA 91109, USA
[6]NOAA ESRL Global Monitoring Division, 325 Broadway, Boulder, CO 80305, USA
[7]CIRES, University of Colorado Boulder, Boulder, CO 80309, USA

[8]School of Life Sciences, Arizona State University, P.O. Box 874501, Tempe, AZ 85287, USA
[9]Earth Atmospheric Sciences, Jet Propulsion Laboratory, 4800 Oak Grove Dr., Pasadena, California 91109, USA

Received: 20 January 2012 – Accepted: 7 February 2012 – Published: 22 February 2012

Correspondence to: S. Newman (sally@gps.caltech.edu)

Published by Copernicus Publications on behalf of the European Geosciences Union.

Abstract

Attributing observed CO_2 variations to human or natural cause is critical to deducing and tracking emissions from observations. We have used in situ CO_2, CO, and planetary boundary layer height (PBLH) measurements recorded during the CalNex-LA (CARB et al., 2008) ground campaign of 15 May–15 June 2010, in Pasadena, CA, to deduce the diurnally varying anthropogenic component of observed CO_2 in the megacity of Los Angeles (LA). This affordable and simple technique, validated by carbon isotope observations, is shown to robustly attribute observed CO_2 variation to anthropogenic or biogenic origin. During CalNex-LA, local fossil fuel combustion contributed up to ~50 % of the observed CO_2 enhancement overnight, and ~100 % during midday. This suggests midday column observations over LA, such as those made by satellites relying on reflected sunlight, can be used to track anthropogenic emissions.

1 Introduction

Climate change induced by increasing anthropogenic greenhouse gas emissions, especially CO_2, is a major societal issue today. It is important to understand the natural variability and emission sources in urban regions, which contribute disproportionately to the atmosphere's anthropogenic greenhouse gas burden (Gurney et al., 2009; Lee et al., 2006; Rayner et al., 2011). The large magnitude of emissions easily detected by elevated concentrations in urban CO_2 domes (Idso et al., 1998; Pataki et al., 2003; Rice and Bostrom, 2011; Rigby et al., 2008) such as Los Angeles (LA), CA (Newman et al., 2008), make megacities important sites for monitoring rapidly changing emissions reflecting rapidly changing natural and anthropogenic processes.

Here we use measurements of CO_2 and CO mixing ratios and planetary boundary layer height (PBLH) collected during the intensive CalNex-LA ground campaign of 15 May–15 June 2010, to demonstrate that ground-based measurements can produce diurnal determinations of the magnitude and source of local CO_2 emissions in a

megacity.

Combustion of fossil fuels is the major local source of both CO and CO_2 in urban environments; however, the biosphere can introduce important sources and sinks for CO_2 (e.g., Pataki et al., 2003), resulting in differences in behavior for the two species. Both components are affected by transport of local and regional air masses to and from the sampling site and by dilution effects due to variations in PBLH. This last is especially important for using surface measurements to validate CO_2 mixing ratios for the total atmospheric column determined by satellite-borne instruments, which will be used to monitor ongoing emissions world-wide.

2 Sampling location and methods

The CalNex-LA site, on the campus of the California Institute of Technology in Pasadena (Fig. 1), is a good location for sampling LA basin emissions because long-lived components tend to be transported inland toward the San Gabriel Mountains, ~4 km to the north, providing an integrated picture of daily emissions in the region. Air masses generally enter the region from the Pacific Ocean, 22 km to the southwest, and flow inland as the sun warms the land and the PBLH increases, exiting the region either through mountain passes or over the mountains by upslope flow or when the PBLH increases sufficiently. The San Gabriel Mountains help to trap nighttime emissions in the basin during most nights, when temperature inversions put a shallow lid on the mixed layer (Lu and Turco, 1994; Neiburger, 1969; Ulrickson and Mass, 1990).

In situ continuous measurements of CO_2 and CO mixing ratios were collected from a 10-m tower near the NE corner of the campus of the California Institute of Technology (Caltech), with ceilometer determinations of PBLH made about 5–10 m away, on the roof a trailer. CO_2 mixing ratios were determined, on a dried air stream, by wavelength-scanned cavity ring-down spectroscopy using a G1101-i Isotopic CO_2 Analyzer from Picarro Instruments (Santa Clara, CA); CO was analyzed by vacuum ultraviolet (VUV) fluorescence using an AL5001 CO instrument from Aero-Laser GmbH

(Garmisch-Partenkirchen, Germany). Planetary boundary layer height was measured by the minimum-gradient method using a Vaisala Ceilometer CL31 (Hamburg, Germany) to determine aerosol backscatter profiles to estimate the PBLH (Münkel et al., 2007). The 10-minute averages for CO_2 and CO mixing ratios and 15-min averages for PBLH were combined into time series of hourly averages. Then campaign-wide averages for each hour were calculated to produce diurnal patterns. (Details regarding analytical methods and calculations are described in Appendices A and B, respectively.)

3 Results

Day-to-day variations of the time series of CO and CO_2 (Fig. 2a) track each other very well. For example, there is a peak on 2-3 June with gradually decreasing mixing ratios over the next eight days and then increasing to the end of the campaign period, roughly inverse to the time series for PBLH (Fig. 2b). Despite these distinct similarities between the CO and CO_2 time series, there are major differences in the averaged hourly diurnal patterns (Fig. 3a), even though they are both long-lived atmospheric components and should be affected similarly by changes in PBLH and advection. The major difference in their behaviors is the influence of the biosphere on CO_2 mixing ratios. Indeed, CO_2 concentrations remain high until sunrise, probably due to respiration of the biosphere, and then are quickly depleted by photosynthesis during the day, with a minimum at ~16:00 (all times in Pacific Standard Time). In contrast, there is a broad maximum in CO, from 08:00–17:00, centered at 12:00, probably due to transport of emissions from LA inland to Pasadena, as the daytime wind speed increases, bringing polluted air from morning rush hour in the basin to the sampling site (Figs. 1b, 3c). A second, smaller peak centered at ~20:00 could reflect afternoon rush hour, on top of an increase in concentration due to development of a shallow temperature inversion layer (Fig. 3b), seen clearly in the diurnal CO_2 pattern (Fig. 3a). CO concentrations decline in the late evening after rush hour subsides, whereas CO_2 values remain high because of the

persistent respiration source. We use these patterns to look at diurnal variations in the magnitude and proportions of the local sources of CO_2.

4 Discussion

4.1 Effect of boundary layer thickness on surface signal

In the simplest view, the boundary layer acts as a box to contain emissions and keep them from mixing with the atmosphere above, concentrating or diluting the emissions as the mixed layer shrinks or deepens, respectively (Holzworth, 1967). This process is a major factor controlling the observed diurnal variations and potentially masking the emissions signal. In addition, we must consider this diurnal change when simulating the column mixing ratios observed by satellite-borne remote-sensing instruments. Reid and Steyn (1997) studied the effect of changing PBLH on CO_2 in Vancouver, BC, including lateral advection and entrainment. Advection is assumed to bring air masses reflecting emissions in the LA basin, based on the relatively local footprint of the site (Fig. 1b). In the simple box model described here, we ignore entrainment and look only at the simpler dilution effects, due to low wind speeds (Fig. 3c) and evidence from aircraft profiles (Fig. A1). We assume that it is the excess over the background mixing ratios (Fig. A2), not the underlying background, that is affected by changing boundary layer depth (inset to Fig. 3a). As expected, the PBLH is greatest during midday (Fig. 3b), when warming inland air rises, increasing wind speed as air is drawn in from the ocean, and disrupts the shallow, stable inversion layer established overnight. We used PBLH measured by ceilometer to determine the mixed layer depth, as corroborated by profiles measured aboard the NOAA P3 aircraft (Fig. A1). In order to calculate the column mixing ratios from those measured on the surface, we must account for the changing size of the mixed layer. We determined the fraction of the atmosphere contained in the boundary layer (details in Appendix B2), which ranges from ~0.03 overnight to ~0.10 midday (inset to Fig. 3b). The resulting contributions to the column

CO_2 and CO for both weekdays and weekend days are 0.8–1.8 ppm CO_2 and 4–21 ppb CO, from nighttime to midday, (inset to Fig. 3d). Although only a small fraction of the atmosphere is contained in the PBL, the magnitude of the emissions is large enough that variations within the PBL are discernable in total column observations. Indeed, they are large enough to be easily observable by satellites, such as the planned Orbiting Carbon Observatory 2 (OCO-2; Miller et al., 2007) observing during the early afternoon.

When these contributions are added to the background mixing ratios (393.1 ppm CO_2 and varying CO of ∼110–135 ppb; Fig. A2), the amplitude and timing of the diurnal patterns (Fig. 3d) for each component are consistent with column mixing ratios observed by an upward pointing Fourier transform spectrometer (FTS) in spring of 2008 for the Pasadena area (at NASA's Jet Propulsion Laboratory (JPL), ∼5 km northwest of Caltech) by Wunch et al. (2011) (Fig. B1), supporting the assumptions that entrainment has negligible influence and concentration variations both within and above the PBL are minor compared to the perturbation due to surface emissions. Although, this pattern has indeed been previously observed (Wunch et al., 2009, 2011), this is the first instance of its report based on much less costly surface measurements. These diurnal patterns for the total atmospheric column (Fig. 3d) are significantly different from those measured at the surface (Fig. 3a) because there is a three-fold change in PBLH, which overwhelms the two-fold changes in the mixing ratio excesses above background. The broad midday peak for each species reflects anthropogenic emissions within the LA basin. CO is known to have virtually no natural sources in urban environments, but to result from incomplete combustion of fossil fuels (e.g., Chinkin et al., 2003), and therefore can be used to attribute CO_2 enhancements to fossil fuel combustion.

4.2 Sources of local CO_2 emissions

Indeed, several studies (Gamnitzer et al., 2006; Levin et al., 2003; Turnbull et al., 2011; 2006; Vogel et al., 2010) have demonstrated that the ratio of the amounts of CO and CO_2 in excess of natural abundances (denoted as COxs and CO_2xs, respectively) can

be used to determine the fraction of CO_2 derived from burning fossil fuels, denoted as F. Although this technique is not as successful as using radiocarbon to differentiate these sources, it is much more practical for use with continuous measurements than the more expensive and time-consuming $\Delta^{14}CO_2$ method (Vogel et al., 2010). A major assumption that must be made when determining F is the value of the CO/CO_2 emission ratio, denoted as R, here assumed to be constant over the time period of the campaign, although it probably does vary (Vogel et al., 2010). Djuricin et al. (2010) concluded that there is much uncertainty in R and therefore only very approximate values of F can be determined. They used R of 0.028 for data collected in Irvine, ∼ 60 km SSE of Pasadena. Wunch et al. (2009) determined R in Pasadena to be 0.011±0.002, using FTS, consistent with R from the California Air Resources Board for southern California (CARB, 2008) and significantly lower than that indicated by the EDGAR inventory (EDGAR, 2009). This value agrees with R calculated for the Sacramento area (Turnbull et al., 2011) using $\Delta^{14}CO_2$ and CO measurements.

COxs/CO_2xs ratios for the CalNex-LA data show a very distinctive diurnal variation (Fig. 4a), being lowest in the early morning (0.005) and highest in the early afternoon (0.012). We averaged the ratios for each hour to investigate the variation of F in Pasadena. Using R determined by Wunch et al. (2009) (0.011±0.002), the resulting diurnal pattern (Fig. 4b) shows a maximum value for F within error of 1.0 during midday. At night, this analysis suggests that 50% of the local contribution is from anthropogenic combustion of fossil fuels. The other 50 % presumably comes from soil and plant respiration. The stable, shallow nighttime PBL (Fig. 3b) traps daytime emissions, so that F never falls much below 50%, even though the dominant source (motor vehicle exhaust) decreases significantly during this time. The amount of CO_2 contributed by fossil fuels ranges from 12 to 21 ppm overnight to midday, respectively, and by the biosphere from a sink of ≤2 ppm during midday to a source of 17 ppm during early morning (Fig. 4c). One might presume that urban regions never experience significant biogenic CO_2 emissions. However, this night-time result of ∼50% CO_2ff (Fig. 4b) is consistent with $\Delta^{14}CO_2$ results from February-March, 2005, for Pasadena (Affek et al.,

2007), for which 36 % of the local CO_2 contribution was attributed to biosphere respiration. During late spring, for the CalNex-LA campaign, it is reasonable to expect an even larger proportion of the night-time emissions to be from respiration, since there is even more biomass during this late spring time period. And significant respiration at night has been observed during spring and late summer/early fall in Salt Lake City, UT (Pataki et al., 2003).

The validity of the major assumption of constant R needs to be evaluated, since it has implications as to the importance of the biosphere in contributing CO_2 emissions in this urban environment. As a sensitivity test, we consider the case where F is constrained to be 1 throughout the diurnal cycle. In this case, R must vary from <0.005 in the early morning hours to 0.012 during midday. A value as low as 0.005 has not been observed for urban regions (e.g., Bishop and Stedman, 2008). Since the unreasonably low value of R required to ensure no biogenic CO_2 input applies to the early hours of the morning (3:00-4:00), we conclude that at this time of day there must have been a significant contribution from the biosphere. Although we cannot provide a direct measure of R for this time period, we suggest that our assumed constant value of 0.011±0.002 is reasonable, since it agrees with the lower limit in Heidelberg (Vogel et al., 2010) and the lowest value derived from the data of Bishop et al. (2008; 0.009).

Data from other methods are available to confirm the results from the CO/CO_2 data during midday. First, two measurements were made for $\Delta^{14}CO_2$ of CO_2 aggregated from flask samples collected at 14:00 on alternate days 17–29 May (−6.4±1.6‰) and 31 May–14 June (−20.6±1.3‰) (Appendix A5). These $\Delta^{14}CO_2$ measurements indicate values for F of 0.9±0.1–1.1±0.1 (corresponding to 1.0±0.1–1.1±0.1 by the COxs/CO_2xs analysis for the same hours as the $\Delta^{14}CO_2$ samples) and 18±3–24±3 ppm CO_2 contributions (15±3–17±2 ppm for the COxs/CO_2xs analysis) for the average 14:00 hour (Fig. 4c) in the early and late halves of the CalNex-LA period, respectively, consistent with the CO/CO_2 results. Second, the daytime result is also consistent with mass balance calculations of $\delta^{13}C$ and CO_2 for flasks collected at 14:00 during 2002–2003, which indicated that F of 0.8–1.0 could explain the observed sta-

ble isotopic composition (Newman et al., 2008). Third, the CO-based estimate of fossil fuel CO_2 agrees well (RMS difference ∼ 5 ppm) with predicted afternoon fossil fuel CO_2 signals calculated using WRF-STILT footprints combined with the Vulcan 2.0 fossil fuel inventory (see Appendix B4; Figs. B2 and B3). Together, these different approaches confirm that high-precision measurements of CO and CO_2, combined with appropriate background measurements and determination of R, can give meaningful diurnal variation of local sources of fossil fuel CO_2.

5 Conclusion

Attribution remains a central challenge to carbon cycle science. Here we have combined two known approaches, looking at CO/CO_2 ratios and using PBLH with a simple box model, and demonstrated a simple and affordable technique to diurnally differentiate anthropogenic and natural components of CO_2 observed in LA. CO_2 enhancements observed during May–June, 2010 were composed of ∼100 % emissions from combustion of fossil fuels during the middle of the day, reducing to ∼50% at night. These ratios were determined by diurnal variations of CO/CO_2 ratios and confirmed for 14:00 by $\Delta^{14}CO_2$. CO_2 from the biosphere varies dramatically, from being a source of ∼17 ppm at 04:00 to a sink of ≤2 ppm at 11:00–12:00. Deployment of sensors to monitor CO_2, CO, and PBLH throughout a megacity such as LA would provide invaluable attribution information. There are also implications of our results for remote sensing of CO_2 from space, as midday column signals, large enough to see with an OCO-like sensor (Miller et al., 2007), can be attributed to anthropogenic activities and tracked over time.

Appendix A

Analytical methods

A1 Site description

As with all cities, there are a few trees nearby and there are surface streets surrounding the block of the campaign site. The closest highway is ∼1 km to the north. Although the closest power plant, Caltech's cogeneration plant, is ∼1 km SW of the site, its combustion products cannot be producing the trends we observed, since its fuel consumption is constant over time.

A2 Analyses of CO_2 mixing ratios

We determined CO_2 mixing ratios by wavelength-scanned cavity ring-down spectroscopy using a G1101-i Isotopic CO_2 Analyzer from Picarro Instruments (Santa Clara, CA). Air CO_2 values were measured after passing the sample stream through $Mg(ClO_4)_2$ to remove H_2O. The values reported are averages of consecutive 10-min periods of 5-min running averages of measurements taken every ∼8 s. The instrument was calibrated daily for CO_2 using three dry air standard tanks from NOAA, with each gas run for 30 min. The standards contained 378.87±0.03, 415.15±0.06, and 493.74±0.03 ppm, respectively. The calibration line for each day was determined by regression of standard values determined by the average of 10 min of 5-min running averages after purging the instrument with each standard for 15 min. The average uncertainty for the CO_2 mixing ratio measurements was ±0.08 ppm.

We used data from a site on Palos Verdes Peninsula (33.74° N 118.35° W; 335 m above sea level) to determine CO_2 background mixing ratios for calculations described below. Data were collected every 20 seconds by a CIRAS-SC (PP Systems, Amesbury, MA) non-dispersive infrared gas analyzer after passing through $Mg(ClO_4)_2$ to dry the air stream. This instrument maintains stability by running a zero every 30 min. The

span of the instrument was calibrated twice a week using a standard air tank from NOAA (420.18±0.03 ppm). The average uncertainty was ±0.5 ppm. The data from this site are shown in Fig. A2a.

A3 Analysis of CO mixing ratios

CO was analyzed by vacuum ultraviolet fluorescence using an AL5001 CO instrument from Aero-Laser GmbH (Garmisch-Partenkirchen, Germany). The analytical method is based on the fluorescence of CO at 150 nm (Gerbig et al., 1999). The sources of calibration uncertainty includes the uncertainty of the NIST (National Institute of Standards and Technology) traceable calibration gas mixture (±2%) from Scott Marrin, Inc. (Riverside, CA) and the uncertainty of repeatability from the standard deviation of the slopes (±3.7 %) from twenty nine daily calibrations. The combined uncertainty was estimated through propagation of the uncertainties as $((d_1)^2 + (d_2)^2 + (d_n)^2)^{1/2}$ with d_n defined as any individual uncertainty (e.g. calibration standard, repeatability, pressure, etc.) and was estimated ±4.2% (Taylor and Kuyatt, 1996). The detection limit was 9.8 ppbv (1σ) based on integration time of 10 s data. For CO, averages of 10 minutes of data collected every 10 s are presented in this paper.

A4 Planetary boundary layer height determination

Planetary boundary layer height was measured by the minimum-gradient method using a Vaisala Ceilometer CL31 (Hamburg, Germany) to determine aerosol backscatter profiles to estimate the PBLH (Münkel et al., 2007). This method assumes the aerosol gradient is a result of a temperature inversion associated with the entrainment zone, which marks the boundary between PBL and free tropospheric air (Emeis and Schäfer, 2006; Schäfer et al., 2004). Please refer to Haman (2011) for a detailed description of the instrument and settings used in this study. An overlap correction was not applied to the reported PBLH. The average uncertainty was ±5 m for the PBLH, and the lowest detectable PBLH of the ceilometer was 80 m due to height averaging constraints. Pre-

vious studies show overall agreement between ceilometer, radiosonde, and SODAR (Sonic Detection And Ranging) estimated PBLHs during both stable and unstable conditions (e.g., Haman, 2011; Martucci et al., 2007; Münkel et al., 2007; van der Kamp and McKendry, 2010). Additionally, Haman et al. (2012) showed only a small bias (-23 m) between ceilometer and ozone profile estimates of the PBL height, which indicates collocation of the ozone and aerosol defined mixed layer height.

Four aircraft profiles were flown over the CalNex-LA ground site on 16 and 19 May 2010 (1 and 3 profiles, respectively; Fig. A1), extending from within the boundary layer into the free troposphere. Temperature and various chemical species, including CO and CO_2, were measured. Airborne CO measurements were provided by vacuum UV resonance fluorescence, with accuracy of ±5 % and precision of ±1 ppb (Holloway et al., 2000); airborne CO_2 measurements were provided by wavelength- canned cavity ring down spectroscopy (model 1301-m, Picarro Instruments, Sunnyvale, CA; Chen et al., 2010), with accuracy of ±0.10 ppm and precision of ±0.15 ppm.

A5 ^{14}C analysis

CO_2 was cryogenically extracted from air collected at 14:00 on alternate afternoons in evacuated 1-liter Pyrex flasks (Newman et al., 2008). Two weeks' samples (7–8 flasks) were combined to produce two CO_2 samples for ^{14}C analysis, for the first and second halves of the CalNex-LA campaign (17–29 May and 31 May–14 June 2010). The CO_2 was graphitized using the sealed tube zinc reduction method (Khosh et al., 2010; Xu et al., 2007). ^{14}C analysis was conducted at the Keck Carbon Cycle AMS facility at the University of California, Irvine (KCCAMS), where the system is a compact accelerator mass spectrometer (AMS) from National Electrostatics Corporation (NEC 0.5MV 1.5SDH-2 AMS system) with a modified NEC MC-SNIC ion-source (Southon and Santos, 2004, 2007). The in-situ simultaneous AMS $\delta^{13}C$ measurement at KCCAMS allowed for the correction of fractionation that occurred both during the graphitization process and inside the AMS system, and thus significantly improved the precision and accuracy of our measurements. The relative error of our day-to-day analysis, including

extraction, graphitization and AMS measurement, is 2.5–3.1‰ based on our secondary standards processed during the past few years.

Appendix B

Data analysis calculations

B1 Averaging and backgrounds

Hourly averages were calculated for CO_2, CO, and PBLH measurements, respectively, through the time period of the CalNex-LA ground campaign. The diurnal patterns shown in Fig. 3 of the main text were produced by first generating hourly time series from the 10–15-min averages and then averaging the individual hours for all days of the campaign.

We determined the excess CO_2 and CO by subtracting the background concentrations for each component. We assumed that the background mixing ratios and isotopic values were constant for CO_2 and $\Delta^{14}C$ and time-varying for CO and reflected representative marine boundary layer values. For CO_2, we subtracted the average of the daily minima for Palos Verdes for the CalNex-LA time period (393.1 ppm; Fig. A2a), which is consistent with measurements for the free troposphere as measured by the NOAA P3 aircraft (Fig. A1); for CO, we subtracted the time-varying average from the NOAA marine boundary layer curtain (extrapolated into the vertical dimension from the GLOBALVIEW curtain (GLOBALVIEW-CO, 2009) appropriate for each hour, as determined by back trajectories calculated using the WRF-STILT (Fig. A2b). The CO background mixing ratios varied from ∼135 ppb in the beginning of the time period to ∼112 ppb on 6 June, and ∼110 ppb at the end of the campaign. The diurnal patterns for the local contributions, in excess of the background values, are shown in the inset to Fig. 3a of the main text.

The background composition for $\Delta^{14}CO_2$ was taken to be 35.5±2‰, derived from extrapolation of data for La Jolla (Graven et al., 2012) to 31 May 2010. This value was used in the calculation of the fraction of CO_2 added locally as fossil fuels, using equation 1 of Turnbull et al. (Turnbull et al., 2011) and assuming no significant contribution from other sources such as biomass burning and heterotrophic respiration.

B2 Conversion of planetary boundary layer heights to pressure

For each hour of the campaign, the PBLH data were converted to pressure using a form of the hydrostatic equation assuming a constant lapse rate:

$$P = P_0 \cdot \left[1 - \frac{L \cdot h}{T_0}\right]^{\frac{-g}{L \cdot R}} \quad \text{(B1)}$$

where P is pressure (Pa), P_0 is the standard pressure at sea level (101,325 Pa), L is the lapse rate near the surface ($-0.0065\,K\,m^{-1}$), T_0 is the standard temperature of 288.15 K, R is the gas constant for air ($287.053\,J\,(kg^{-1}\,K^{-1})$), and h is altitude above sea level (m) (US Standard Atmosphere, 1976; Wallace and Hobbs, 1977). The fraction of the atmosphere contained in the boundary layer was calculated as the ratio of the difference between the pressures at the top and bottom of the boundary layer to the pressure at the surface (($P_{246\,m}$–P_{PBLH})/$P_{246\,m}$; where $P_{246\,m}$ is the pressure at the level of the in-situ surface measurements at 246 m above sea level and P_{PBLH} is the pressure at the top of the mixed layer). This fraction was multiplied by the surface mixing ratios of CO_2 and CO in excess of the background values to produce the amount of each component that was added to the total atmospheric column above Pasadena and then averaged for each hour of the day for weekdays and weekends, respectively (inset to Fig. 3d). This approach assumes no entrainment during the diurnal cycle of increasing and decreasing PBLH. Indeed lack of significant entrainment is confirmed by aircraft profile made over the sampling site during the campaign (Fig. A1), which show that the transition from the mixed layer to the overlying free troposphere is thin, less than

500 m thick for the four profiles showing it on 16 and 19 May 2010. The magnitude of variation of the diurnal patterns calculated here agree with those determined during May–June 2008 by Fourier transform spectroscopy (FTS) at NASA's Jet Propulsion Laboratory (JPL) ∼5 km to the NW of the CalNex-LA site (Fig. B1; Wunch et al., 2011). This agreement supports the adoption of these simplifying assumptions.

B3 Footprint calculations

The footprint (sensitivity of observation to surface emissions) was calculated using the Stochastic Time-Inverted Lagrangian Transport Model (STILT; Lin et al., 2003), driven by time-averaged mass fluxes generated by the Weather Research and Forecasting Model (WRF; Nehrkorn et al., 2010). For the initial STILT calculations to determine the time-averaged footprint, 100 particles are released from the observation site at 13:00 local time for 15 May–15 June 2010. These particles are tracked as they move backward in time, stochastically sampling the turbulence, and the footprint can be calculated from the particle density and residence time in the layer which sees surface emissions, defined as 0.5 PBLH (see citations for more details on STILT and STILT-WRF). Footprint findings demonstrate the Caltech site is well situated for sampling the emissions signal from the LA basin. Based on this observation, we conclude that the effective sampling region comprises the LA basin, and that there is no major advective transport into the basin besides that of ocean breezes.

B4 Prediction of atmospheric fossil fuel signals

Predicted fossil fuel CO_2 (CO_2ff) mixing ratio signals were calculated using spatially and temporally resolved a priori CO_2ff emissions and WRF-STILT footprints. Comparisons between model results and measurements for CO_2ff are shown in Fig. B2 and B3a and for PBLH in Fig. B3b. The WRF runs follow methods applied by Zhao et al. (2009) for California methane, with modifications that included use of the Mellor-Yamada-Janjic (MYJ) boundary layer scheme (Janjic, 1990; Mellor and Yamada, 1982),

nested sub-domains using spatial resolutions of 36 km, 12 km, and 4 km with 50 vertical layers, and two-way nesting from each outer sub-region. Evaluation of predicted boundary layer depths were compared with the ceilometer measurements. STILT footprints were calculated using 500 particles. Fossil fuel CO_2 emissions were obtained at hourly temporal and 10 km spatial resolution from the VULCAN2.0 inventory. (http://vulcan.project.asu.edu/index.php).

Acknowledgements. We appreciate productive discussions with Paul Wennberg, Michael Line, Xi Zhang, Run-Lie Shia, and Joshua Kammer. WRF winds for the time-averaged footprints during the CalNex period were provided by Wayne Angevine (NOAA). John S. Holloway (NOAA) provided the measurements of CO from the P3 aircraft profiles. As part of the CalNex-LA campaign, we gratefully acknowledge the support of Caltech and the California Air Resources Board in making the campaign successful. SN acknowledges financial support from JPL's Director's Research and Development Fund. Analysis by MLF and SJ was supported by the Director, Office of Science, of the US Department of Energy under Contract No. DE-AC02-05CH11231.

References

Affek, H., Xu, X., and Eiler, J.: Seasonal and diurnal variations of $^{13}C^{18}O^{16}O$ in air: Initial observations from Pasadena, CA, Geochim. Cosmochim. Acta, 71, 5033–5043, 2007.

Bishop, G. A. and Stedman, D. H.: A decade of on-road emissions measurements, Environ. Sci. Technol., 42, 1651–1656, doi:10.1021/es702413b, 2008.

California Air Resources Board (CARB): California emission inventory data almanac, technical report, available online at: http://www.arb.ca.gov/app/emsinv/emssumcat.php, 2008.

California Air Resources Board (CARB), National Oceanic and Atmospheric Administration (NOAA) and California Energy Commission (CEC): CalNex White Paper: Research at the Nexus of Air Quality and Climate Change, 1–12, available online at: http://www.arb.ca.gov/research/fieldstudy2010/calnexus_white_paper_01_09.pdf, 2008.

Chen, H., Winderlich, J., Hoefer, A., Rella, C. W., Crosson, E., Van Pelt, A. D., Steinbach, J., Kolle, O., Beck, V., Daube, B. C., Gottlieb, E. W., Chow, V. Y., Santoni, G. W., and Wofsy, S. C.: High-accuracy continuous airborne measurements of greenhouse gases (CO_2 and

CH_4) using the cavity ring-down spectroscopy (CRDS) technique, Atmos. Meas. Tech., 3, 375–386, doi:10.5194/amt-3-1113-2010, 2010.

Chinkin, L. R., Coe, D. L., Funk, T. H.,Hafner, H. R., Roberts, P. T., Ryan, P. A., and Lawson, D. R.: Weekday versus weekend activity patterns for ozone precursor emissions in California's South Coast Air Basin, J. Air & Waste Manage. Assoc., 53, 829–843, 2003.

Djuricin, S., Pataki, D. E., and Xu, X.: A comparison of tracer methods for quantifying CO_2 sources in an urban region, J. Geophys. Res.-Atmos., 115, D11303, doi:10.1029/2009JD012236, 2010.

EDGAR Project Team: Emission database for global atmospheric research (EDGAR), release version 4.0., http://edgar.jrc.ec.europa.eu/index.php, Eur. Comm. Joint Res. Cent., Brussels, 2009.

Emeis, S. and Schäfer, K.: Remote sensing methods to investigate boundary-layer structures relevant to air pollution in cities, Bound.-Lay. Meteorol., 121, 377–385, doi:10.1007/s10546-006-9068-2, 2006.

Gamnitzer, U., Karstens, U., Kromer, B., Neubert, R. E. M., Meijer, H. A. J., Schroeder, H., and Levin, I.: Carbon monoxide: A quantitative tracer for fossil fuel CO_2?, J. Geophys. Res.-Atmos., 111, D22302, doi:10.1029/2005JD006966, 2006.

Gerbig, C., Schmitgen, S., Kley, D., Volz-Thomas, A., Dewey, K., and Haaks, D.: An improved fast-response vacuum-UV resonance fluorescence CO instrument, J. Geophys. Res.-Atmos., 104, 1699–1704, 1999.

GLOBALVIEW-CO: Cooperative Atmospheric Data Integration Project – Carbon Monoxide, CD-ROM, NOAA ESRL, Boulder, Colorado, also available on Internet via anonymous FTP to ftp.cmdl.noaa.gov, Path: ccg/co/GLOBALVIEW], 2009.

Graven, H. D., Guilderson, T. P., and Keeling, R. F.: Observations of radiocarbon in CO_2 at La Jolla, California, USA 1992–2007: Analysis of the long-term trend, J. Geophys. Res.-Atmos., 117, D02302, doi:10.1029/2011JD016533, 2012.

Gurney, K. R., Mendoza, D. L., Zhou, Y., Fischer, M. L., Miller, C. C., Geethakumar, S., and de la Rue du Can, S.: High Resolution Fossil Fuel Combustion CO_2 Emission Fluxes for the United States, Environ. Sci. Technol., 43, 5535–5541, 2009.

Haman, C. L.: Seasonal and daily variability of the boundary layer and the impact of synoptic controls and micrometeorological processes on surface ozone evolution at an urban site, Ph.D. thesis, University of Houston, Texas, USA, 2011.

Haman, C. L., Lefer, B. L., and Morris, G. A.: Seasonal variability in the diurnal evolution of the

boundary layer in a near coastal urban environment, J. Atmos. Ocean. Technol., JTECH-D-11-00114, in press, 2012.

Holloway, J. S., Jakoubek, R. O., Parrish, D. D., Gerbig, C., Volz-Thomas, A., Schmitgen, S., Fried, A., Wert, B., Henry, B., and Drummond, J. R.: Airborne intercomparison of vacuum ultraviolet fluorescence and tunable diode laser absorption measurements of tropospheric carbon monoxide, J. Geophys. Res.-Atmos., 105, 24251–24261, 2000.

Holzworth, G. C.: Mixing depths, wind speeds and air pollution potential for selected locations in the United States., J. Appl. Meteorol., 6, 1039–1044, 1967.

Idso, C. D., Idso, S. B., and Balling, R. C.: The urban CO_2 dome of Phoenix, Arizona, Phys. Geogr., 19, 95–108, 1998.

Janjic, Z. I.: The step-mountain coordinate – physical package, Mon. Weather Rev., 118, 1429–1443, 1990.

Khosh, M. S., Xu, X., and Trumbore, S. E.: Small-mass graphite preparation by sealed tube zinc reduction method for AMS C-14 measurements, Nucl. Instrum. Meth. B, 268, 927–930. 2010.

Lee, B. H., Munger, J. W., Wofsy, S. C., and Goldstein, A. H.: Anthropogenic emissions of nonmethane hydrocarbons in the northeastern United States: Measured seasonal variations from 1992–1996 and 1999–2001, J. Geophys. Res.-Atmos., 111, D20307, doi:10.1029/2005JD006172, 2006.

Levin, I., Kromer, B., Schmidt, M., and Sartorius, H.: A novel approach for independent budgeting of fossil fuel CO_2 over Europe by $^{14}CO_2$ observations, Geophys. Res. Lett., 30, 2194, doi:10.1029/2003GL018477, 2003.

Lin, J. C., Gerbig, C., Wofsy, S. C., Andrews, A. E., Daube, B. C., Davis, K. J., and Grainger, C. A.: Near-field tool for simulating the upstream influence of atmospheric observations: The Stochastic Time-Inverted Lagrangian Transport (STILT) model, J. Geophys. Res.-Atmos., 108, 4493, doi:10.1029/2002JD003161, 2003.

Lu, R. and Turco, R. P.: Air pollutant transport in a coastal environment. Part I: Two-dimensional simulations of sea-breeze and mountain effects, J. Atmos. Sci., 51, 2285–2308, 1994.

Martucci, G., Matthey, R., Mitev, V., and Richner, H.: Comparison between backscatter lidar and radiosonde measurements of the diurnal and nocturnal stratification in the lower troposphere, J. Atmos. Ocean. Technol., 24, 1231–1244, doi:10.1175/JTECH2036.1, 2007.

Mellor, G. L. and Yamada, T.: Development of a turbulence closure model for geophysical fluid problems, Rev. Geophys. Space Phys., 20, 851–875, 1982.

Miller, C. E., Crisp, D., DeCola, P. L., Olsen, S. C., Randerson, J. T., Michalak, A. M., Alkhaled, A., Rayner, P., Jacob, D. J., Suntharalingam, P., Jones, D. B. A., Denning, A. S., Nicholls, M. E., Doney, S. C., Pawson, S., Boesch, H., Connor, B. J., Fung, I. Y., O'Brien D., Salawitch, R. J., Sander, S. P., Sen, B., Tans, P., Toon, G. C., Wennberg, P. O., Wofsy, S. C., Yung, Y. L., and Law, R. M.: Precision requirements for space-based X-CO_2 data, J. Geophys. Res.-Atmos., 112, D10314, doi:10.1029/2006JD007659, 2007.

Münkel, C., Eresmaa, N., Räsänen, J., and Karppinen, A.: Retrieval of mixing height and dust concentration with lidar ceilometer, Bound.-Lay. Meteorol., 124, 117–128, doi:10.1007/s10546-006-9103-3, 2007.

Nehrkorn, T., Eluszkiewicz, J., Wofsy, S. C., Lin, J. C., Gerbig, C., Longo, M., and Freitas, S.: Coupled weather research and forecasting-stochastic time-inverted lagrangian transport (WRF-STILT) model, Meteorol. Atmos. Phys., 107, 51–64, doi:10.1007/s00703-010-0068-x, 2010.

Neiburger, M.: The role of meteorology in the study and control of air pollution, B. Am. Meteorol. Soc., 50, 957–965, 1969.

Newman, S., Xu, X., Affek, H. P., Stolper, E., and Epstein, S.: Changes in mixing ratio and isotopic composition of CO_2 in urban air from the Los Angeles basin, California, between 1972 and 2003, J. Geophys. Res.-Atmos., 113, D23304, doi:10.1029/2008JD009999, 2008.

Novelli, P. C., Elkins, J. W., and Steele, L. P.: The development and evaluation of a gravimetric reference scale for measurements of atmospheric carbon monoxide, J. Geophys. Res.-Atmos., 96, 13109–13121, 1991.

Pataki, D. E., Bowling, D. R., and Ehleringer, J. R.: Seasonal cycle of carbon dioxide and its isotopic composition in an urban atmosphere: Anthropogenic and biogenic effects, J. Geophys. Res.-Atmos., 108, 4735, doi:10.1029/2003JD003865, 2003.

Rayner, P. J., Raupach, M. R., Paget, M., Peylin, P., and Koffi, E.: A new global gridded data set of CO_2 emissions from fossil fuel combustion: Methodology and evaluation, J Geophys. Res.-Atmos., 115, D19306, doi:10.1029/2009JD013439, 2010.

Reid, K. H. and Steyn, D. G.: Diurnal variations of boundary-layer carbon dioxide in a coastal city – observations and comparison with model results, Atmos. Environ., 31, 3101–3114, 1997.

Rice, A. and Bostrom, G.: Measurements of carbon dioxide in an Oregon metropolitan region, Atmos. Environ., 45, 1138–1144, doi:10.1016/j.atmosenv.2010.11.026, 2011.

Rigby, M., Toumi, R., Fisher, R., Lowry, D., and Nisbet, E. G.: First continuous measurements

of CO_2 mixing ratio in central London using a compact diffusion probe, Atmos. Environ., 42, 8943–8953, doi:10.1016/j.atmosenv.2008.06.040, 2008.
Schäfer, K., Emeis, S. M., Rauch, A., and Vogt, C.: Determination of mixing layer heights from ceilometer data, Remote Sens. Clouds Atmos. IX, SPIE, 5571, 248–259, 2004.
Southon, J. and Santos, G. M.: Ion source development at KCCAMS, University of California, Irvine, Radiocarbon, 46, 33–39. 2004.
Southon, J. and Santos, G. M.: Life with MC-SNICS. Part II: Further ion source development at the Keck carbon cycle AMS facility, in Nucl. Instrum. Meth. B, 259, 88–93. 2007.
Taylor, B. N. and Kuyatt, C. E.: Guidelines for Evaluating and Expressing the Uncertainty of NIST Measurement Results, NIST Technical Note 1297, 1–25, 1996.
Turnbull, J. C., Karion, A., Fischer, M. L., Faloona, I., Guilderson, T., Lehman, S. J., Miller B. R., Miller, J. B., Montzka, S., Sherwood, T., Saripalli, S., Sweeney, C., and Tans, P. P.: Assessment of fossil fuel carbon dioxide and other anthropogenic trace gas emissions from airborne measurements over Sacramento, California in spring 2009, Atmos. Chem. Phys., 11, 705–721, doi:10.5194/acp-11-705-2011, 2011.
Turnbull, J. C., Miller, J. B., Lehman, S. J., Tans, P. P., Sparks, R. J., and Southon, J.: Comparison of $^{14}CO_2$, CO, and SF_6 as tracers for recently added fossil fuel CO_2 in the atmosphere and implications for biological CO_2 exchange, Geophys. Res. Lett., 33, L01817, doi:10.1029/2005GL024213, 2006.
Ulrickson, B. L. and Mass, C. F.: Numerical investigation of mesoscale circulations over the Los Angeles basin. 1. A verification study, Mon. Weather Rev., 118, 2138–2161, 1990.
US Standard Atmosphere: US Government Printing Office, available online at: http://www.pdas.com/refs/us76.pdf, 1976.
van der Kamp, D. and McKendry, I.: Diurnal and seasonal trends in convective mixed-layer heights estimated from two years of continuous ceilometer observations in Vancouver, BC, Bound.-Lay. Meteorol., 137, 459–475, doi:10.1007/s10546-010-9535-7, 2010.
Vogel, F. R., Hammer, S., Steinhof, A., Kromer, B., and Levin, I.: Implication of weekly and diurnal ^{14}C calibration on hourly estimates of CO-based fossil fuel CO_2 at a moderately polluted site in southwestern Germany, Tellus B, 62, 512–520, doi:10.1111/j.1600-0889.2010.00477.x, 2010.
Wallace, J. M. and Hobbs, P. V.: Atmospheric Science: An Introductory Study, Academic Press, Inc., Orlando, FL, USA, 1977.
Wunch, D., Toon, G. C., Blavier, J. F. L., Washenfelder, R. A., Notholt, J., Connor, B. J., Griffith,

D. W. T., Sherlock, V., and Wennberg, P. O.: The Total Carbon Column Observing Network, Philos. T. Roy. Soc. A, 369, 2087–2112, doi:10.1098/rsta.2010.0240, 2011.
Wunch, D., Wennberg, P. O., Toon, G. C., Keppel-Aleks, G., and Yavin, Y. G.: Emissions of greenhouse gases from a North American megacity, Geophys. Res. Lett., 36, L15810, doi:10.1029/2009GL039825, 2009.
Xu, X., Trumbore, S. E., Zheng, S., Southon, J. R., McDuffee, K. E., Luttgen, M., and Liu, J. C.: Modifying a sealed tube zinc reduction method for preparation of AMS graphite targets: Reducing background and attaining high precision, in Nucl. Instrum. Meth. B., 259, 320–329. 2007.
Zhao, C., Andrews, A. E., Bianco, L., Eluszkiewicz, J., Hirsch, A., MacDonald, C., Nehrkorn, T., and Fischer, M. L.: Atmospheric inverse estimates of methane emissions from Central California, J. Geophys. Res.-Atmos., 114, D16302, doi:10.1029/2008JD011671, 2009.

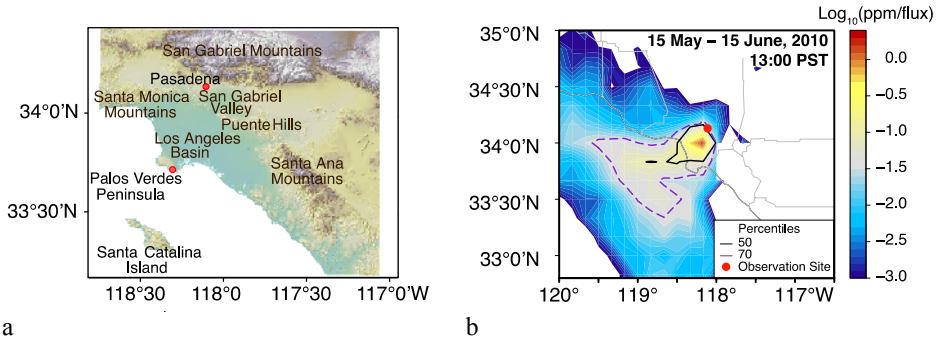

Fig. 1. **(a)** Location of Pasadena in southern California. The sampling location was 34.14° N 118.12° W, 246 m above sea level sampling height, 10 m above ground level. Also shown is the site on Palos Verdes Peninsula where CO_2 was measured for background air (see Appendix A2). **(b)** Average midday footprint for the Caltech campus (see Appendix B3 for a description of the calculation). The color scale indicates the influence of the different locations on the CO_2 measured in Pasadena, in ppm CO_2 in Pasadena/flux (flux in µmole s^{-1} m^{-2}) at the indicated location. Grey lines indicate county boundaries. The dashed purple contour surrounds the area which contributes 70 % of the surface influence on the air sampled at the Caltech site. The shape of this contour reflects the average midday wind direction, from the SW (Fig. 3c). The air sampled in Pasadena comes predominantly from the ocean, adding emissions from the LA basin as it passes over, making Pasadena a good receptor site for the megacity.

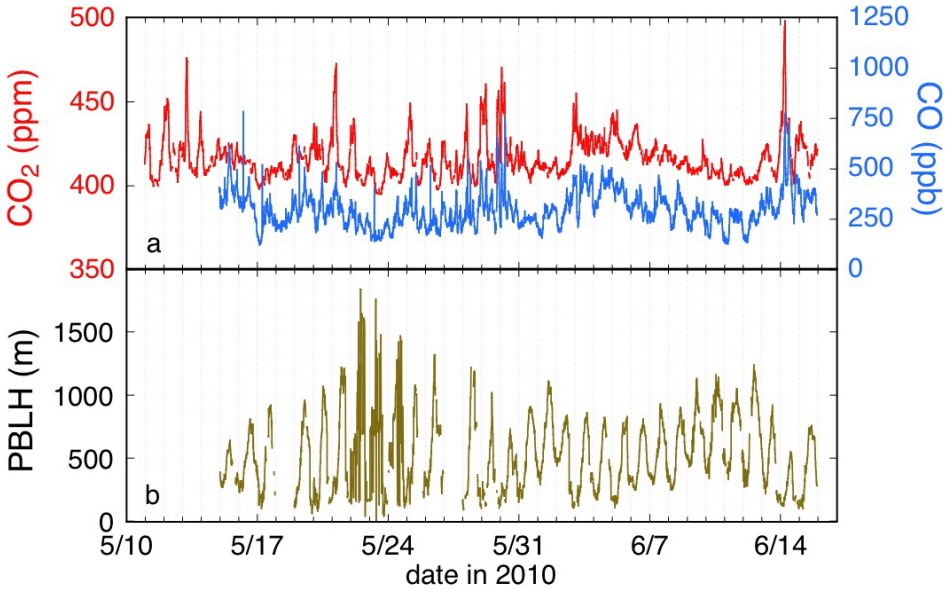

Fig. 2. Time series for the CalNex-LA period for **(a)** CO_2 and CO and **(b)** planetary boundary layer height (PBLH). Measurements plotted are 10-min averages for CO_2 and CO and 15-min averages for PBLH.

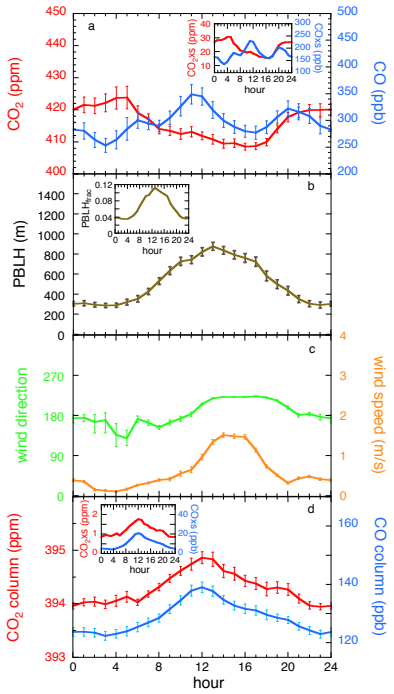

Fig. 3. Average diurnal patterns for weekdays (solid curves) and weekends (dashed curves) for **(a)** measured CO_2 and CO, **(b)** boundary layer height, **(c)** wind speed and direction for non-calm periods, and **(d)** CO_2 and CO in the atmospheric column, after correcting the measured values for changes in boundary layer height. Solid lines indicate data for weekdays, dashed lines for weekends. Insets show **(a)** and **(d)** the excess (xs) CO_2 and CO over background levels (CO_2 background assumed to be constant at 393.1 ppm; CO background taken as time-varying, ranging from 96 to 136 ppb with an average of 115±10 ppb; Appendix B1 and (Novelli et al., 1991) and **(b)** the fraction of the planetary boundary layer relative to the entire atmospheric column (Appendix B2). Error bars indicate standard deviations of the means ($n = 32$).

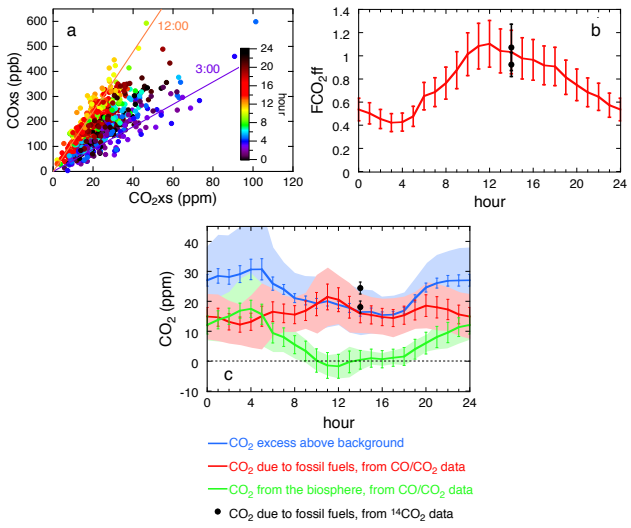

Fig. 4. (a) CO vs. CO_2 in excess of background levels (xs) for hourly averages. Colors indicate time of day. Regression lines for the hours indicated are shown in color. **(b)** Diurnal variation of the fraction of fossil fuels (F) in the local contribution of CO_2 from CO/CO_2xs data shown as purple lines. Black dots indicate data from $\Delta^{14}CO_2$. **(c)** Diurnal cycles, for all days, for CO_2xs (blue), the amount of CO_2 emitted from fossil fuel combustion (CO_2ff; red), and the amount of CO_2 emitted from the biosphere (CO_2bio; green). Black dots indicate data for CO_2ff from $\Delta^{14}CO_2$. Calculations in **(b)** and **(c)** assume an emission ratio of CO/CO_2ff of 0.011±0.002 from Wunch et al. (2009) and backgrounds for CO_2, CO, and $\Delta^{14}CO_2$ as described in Appendix A2. Error bars for F (**b**; red), CO_2ff (**c**; red), and CO_2bio (**c**; green) reflect the error in the emission ratio (18 % relative), for CO_2xs reflect standard errors ($n = 32$), and for CO_2ff from $\Delta^{14}CO_2$ reflect errors in measurements and backgrounds. Shaded regions in c) indicate one standard deviation of the scatter in the hourly averages.

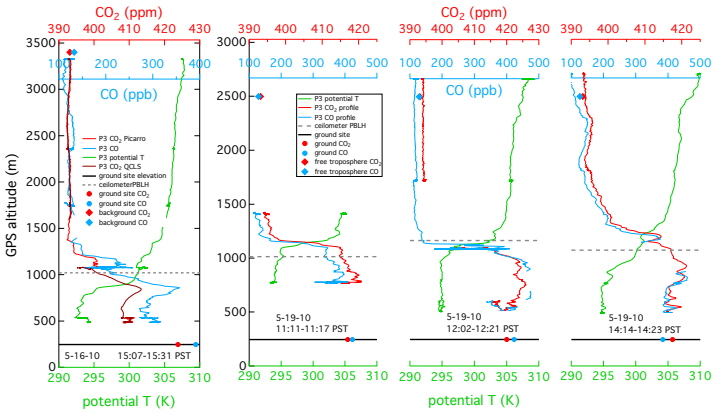

Fig. A1. Profiles of CO_2 (red) and CO (blue) mixing ratios and potential temperature determined by instruments on NOAA's P3 over the CalNex-LA ground site in Pasadena. Circles and diamonds show the compositions of CO_2 (red) and CO (blue) at the ground site and in the free troposphere, respectively. The dashed gray lines indicate the location of the top of the mixed layer determined by the ceilometer at the ground site. These profiles show the rapid transition from PBL to free troposphere and the limited entrainment of PBL CO and CO_2 into the overlying atmosphere, at least for 5/19/10. The maximum PBLH prior to the 5-19-10 at 14:00 profile was 1205 m, whereas the other profiles were collected at the time of the maximum PBLH. Unfortunately, the profiles determined later in the campaign did not extend low enough to intersect the PBL.

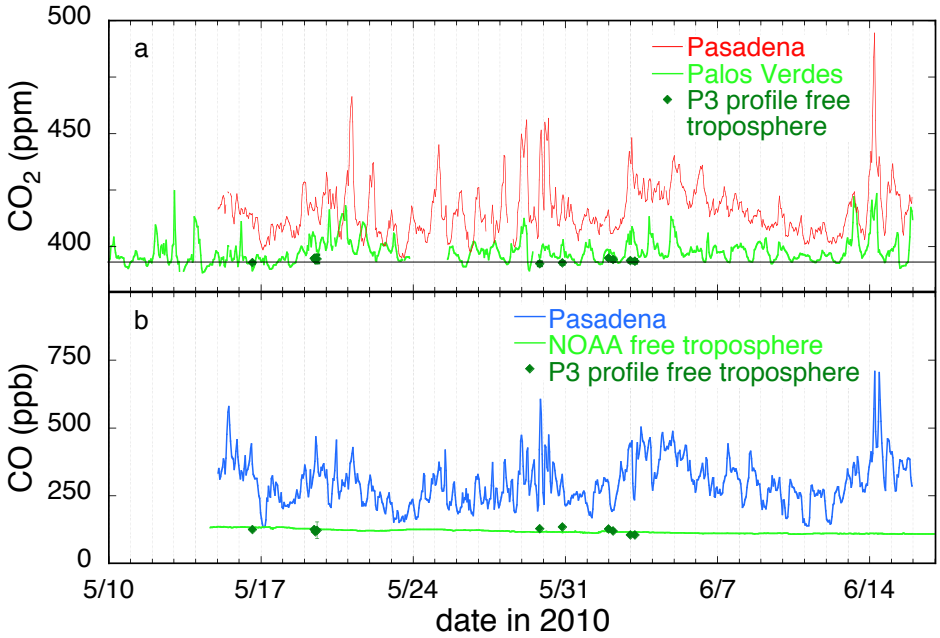

Fig. A2. (a) Time series for CO_2 for the period of the CalNex-LA campaign comparing measurements in Pasadena with those from Palos Verdes peninsula, on a hillside overlooking the ocean. The average daily minimum CO_2 mixing ratio in Palos Verdes of 393.1 ppm, indicated by the horizontal black line, was used for the CO_2 background in all calculations. **(b)** Time series for CO in Pasadena compared with time-varying free tropospheric CO from NOAA curtain (extended into the third dimension from GLOBALVIEW-CO, 2009) and P3 vertical profiles over the Pasadena site.

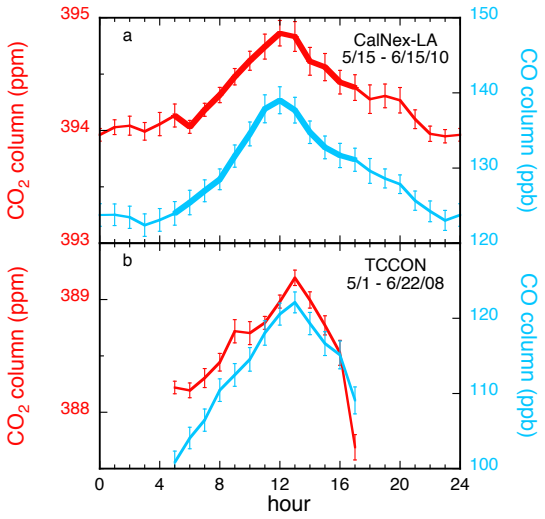

Fig. B1. Comparison of calculated column CO_2 and CO mixing ratios at the CalNex-LA site in May–June 2010 **(a)** with those measured in May–June 2008 at JPL **(b)** by FTS, as part of the Total Carbon Column Observing Network (TCCON; Wunch et al., 2011). Note that CO_2 mixing ratios vary ∼1 ppm and CO ∼15-20 ppb with peaks at 12:00 to 13:00 for both sets of measurements. The thicker lines in **(a)** highlight the hours for which there are data from the FTS. The time period averaged for the TCCON data is longer than for the CalNex-LA data in order to have the same number of data points for the two data sets ($n = 32$, on average). Error bars indicate standard errors.

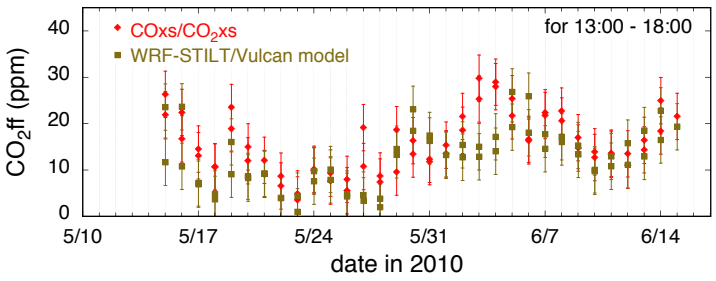

Fig. B2. Comparison of time series for CO_2ff determined using COxs/CO_2xs and constant R of 0.011 with that determined by inverse modeling using WRF-STILT and Vulcan 2.0 emissions, for 13:00–18:00, during the CalNex-LA campaign. For each day, average values are plotted for 13:00–15:00 and 16:00–18:00 for CO_2ff from both measurements and prediction. Error bars are ±5 ppm, based on requiring that reduced $\chi^2 = 1$ during the linear regression calculation.

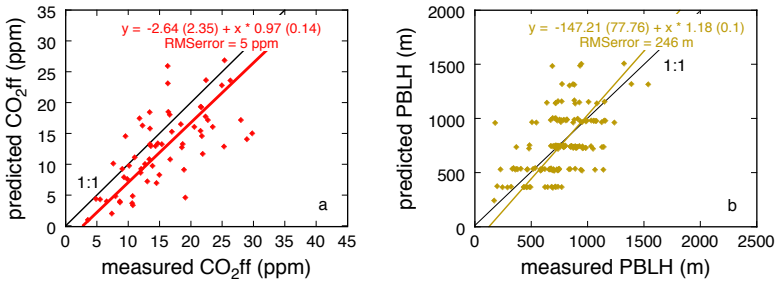

Fig. B3. Direct comparison of predicted versus measured **(a)** CO_2ff and **(b)** PBLH, for 13:00–18:00.